

Constraining the particle production mechanism in Au + Au collisions at $\sqrt{s_{NN}} = 7.7, 27, \text{ and } 200 \text{ GeV}$ using a multiphase transport model

Abhirikshma Nandi,¹ Lokesh Kumar,² and Natasha Sharma²

¹*Indian Institute of Technology Guwahati, Assam, India-781039.*

²*Department of Physics, Panjab University, Chandigarh, India-160014.*

We study the production of pions, kaons, and (anti)protons using a multiphase transport (AMPT) model in Au + Au collisions at $\sqrt{s_{NN}} = 7.7, 27, \text{ and } 200 \text{ GeV}$. We present the centrality and energy dependence of various bulk observables such as invariant yields as a function of transverse momentum p_T , particle yields dN/dy , average transverse momentum $\langle p_T \rangle$, and various particle ratios, and compare them with experimental data. Both default and string melting (SM) versions of the AMPT model are used with three different sets of initial conditions. We observe that neither the default nor the SM version of the model could consistently describe the centrality dependence of all observables at the above energies with any one set of initial conditions. The energy dependence behavior of the experimental observables for 0–5% central collisions is in general better described by the default AMPT model using the modified HIJING parameters for Lund string fragmentation and 3 mb parton scattering cross section. In addition, the kaon production as well as the K/π ratio at 7.7 GeV are under predicted by the AMPT model.

I. INTRODUCTION

Relativistic collisions of heavy ions make it possible to subject nuclear matter to the extreme energy densities required for a possible deconfinement of quarks and gluons. A dense matter with partonic degrees of freedom, often called the quark-gluon plasma (QGP), is expected to form in the initial moments after the collision [1–4]. Exploring the quantum chromodynamics (QCD) phase diagram to understand the properties of quark matter is one of the most important goals of high-energy heavy-ion experiments [5–7]. Comparing the results obtained from theoretical models with the experimental data helps in understanding the space-time evolution of QGP and many of its other properties. The QCD phase diagram is usually plotted as temperature (T) versus baryon chemical potential (μ_B). Assuming a thermalized system is reached in heavy-ion collisions, both T and μ_B can be varied by changing the collision energy [8–10]. To this end, the Beam Energy Scan (BES) program at the BNL Relativistic Heavy Ion Collider (RHIC) completed its first phase of operation in 2010 and 2011 [11–18]. The measurements of the bulk properties of identified hadrons using the BES data were recently published [18]. The measurements from the STAR experiment cover the μ_B interval from 20 to 450 MeV. This is also believed to be the region in which the transition from hadronic matter to QGP takes place [19–25].

In this paper, we have studied Au + Au collisions at $\sqrt{s_{NN}} = 7.7, 27, \text{ and } 200 \text{ GeV}$ using a multi phase transport (AMPT) model and compared bulk properties such as transverse momentum p_T spectra, multiplicity densities dN/dy , average transverse momentum $\langle p_T \rangle$ and particle ratios with the experimental data. For this study we have used three different sets of parameters for both the default and string melting (SM) versions of the AMPT model. It may be noted that comparisons of the elliptic flow v_2 from AMPT with the experimental data from

RHIC BES energies have been done previously [26, 27]. This is, however, the first time that the hadron production has been compared in such detail with the experimental data at these energies. The purpose of this work is to use already tuned parameters for the AMPT model and to see which set of parameters or physics describes the data best and consistently at these energies and different centralities. Thus, we take one parameter set at a time and study its energy and centrality dependence. In total, we consider three different sets, as motivated by previous studies [28–31]. This would help in understanding the particle production in heavy-ion collisions. It may, however, happen that different parameters work at different centralities and/or energies.

The paper is organized as follows. In Section II we give a brief description of the AMPT model and its parameters. In Section III A we present the comparison of transverse momentum spectra between models and experimental data. In Section III B and Section III C we study the centrality dependence of particle yields and average transverse momenta respectively and compare the results with experimental data. The centrality and energy dependence of various particle ratios are discussed in Section III D and Section III E respectively. We summarize in Section IV.

II. THE AMPT MODEL

In this section, we give a short description of the AMPT model and its parameters. The AMPT model was developed to give a coherent description of the dynamics of relativistic heavy-ion collisions [28] and has been used extensively to study them at various energies and environments. It is a hybrid transport model and has four main components: the initial conditions, partonic interactions, hadronization, and hadronic interactions [28]. Initial conditions are obtained from the Heavy Ion Jet In-

teraction Generator (HIJING) model [32]. Hard minijet partons are produced perturbatively if the momentum transfer is more than a threshold ($p_0 = 2 \text{ GeV}/c$) and soft strings are produced otherwise. Depending on the version of AMPT model used, default or string melting, the soft strings are either retained or are completely converted to partons.

Zhangs's parton cascade (ZPC) [33] is used for partonic interactions. The differential scattering cross-section is given by

$$\frac{d\sigma}{dt} \approx \frac{9\pi\alpha_s^2}{2(t - \mu^2)^2}, \quad (1)$$

where σ is the parton-parton scattering cross section, t is the standard Mandelstam variable for four-momentum transfer, α_s is the strong coupling constant, and μ is the Debye screening mass in partonic matter.

In the default model, only the minijet gluons take part in the ZPC and the energy stored in the excited strings is only released after hadrons are formed. For the default model, after the partons stop interacting, they combine with their parent strings. Hadronization of these strings take place using the Lund string fragmentation model [34, 35]. The longitudinal momentum of the hadrons generated is given by the Lund string fragmentation function $f(z) \propto z^{-1}(1-z)^a \exp(-bm_T^2/z)$, z being the light-cone momentum fraction of the hadron of transverse mass m_T with respect to the fragmenting string. The average squared transverse momentum $\langle p_T^2 \rangle$ of the produced particles is proportional to the string tension κ , i.e., the energy stored per unit length of a string, and depends on the Lund string fragmentation parameters as

$$\kappa \propto \langle p_T^2 \rangle = \frac{1}{b(2+a)}. \quad (2)$$

In the string melting version, quarks and antiquarks of all flavors take part in the ZPC, and hadronization takes place via a quark coalescence model in which the nearest partons are combined to form mesons and baryons. The dynamics of the hadronic matter is described by a relativistic transport (ART) model which includes meson-meson, meson-baryon, baryon-baryon, elastic, and inelastic scatterings [36], but the hadronic effects are less important than in the default model. The parton density in ZPC for the SM version is quite high as all HIJING strings are converted to partons. As a result the SM version was found to reasonably fit the elliptic flow at RHIC [28]. It was observed that the SM version could not describe the hadron production, specifically the proton rapidity distributions or the p_T spectra of hadrons [28–30]. However, it was shown in a recent work that an improved quark coalescence could improve the description of hadron production, but more work was needed to be done to improve the baryon and strangeness sector [30].

We have chosen the three tuned parameter sets as given in Table I. Some of these parameters might depend on

TABLE I: Used values of parameters in Lund string fragmentation and parton scattering cross sections for the three sets of AMPT data.

Set	Cross section σ	a	$b \text{ (GeV}^{-2}\text{)}$	α_s	$\mu \text{ (fm}^{-1}\text{)}$
Set A	3 mb	0.55	0.15	0.33	2.265
Set B	1.5 mb	0.5	0.9	0.33	3.2
Set C	10 mb	2.2	0.5	0.47	1.8

the collision conditions, e.g., the Lund fragmentation parameters a and b are expected to depend on the collision centrality. The string tension κ , which depends on a and b , might also be environment dependent due to close packing of strings [37]. In the model, the screening mass μ is a parameter for changing the parton scattering cross sections but it is generated by medium effects. So, a medium dependent screening mass would produce results truer to real physics. Instead of using different parameters for different collision conditions, three sets of constant parameters are used for this study. These have been chosen by taking guidance from earlier studies as detailed below. The parton scattering cross section is given as $\sigma \approx 9\pi\alpha_s^2/(2\mu^2)$. Thus, the value of σ depends on a given combination of α_s and μ . It has been observed that the multiplicity is not very sensitive to the parton scattering cross section σ [31], but σ seems to affect the elliptic flow such that a larger parton scattering cross section leads to large elliptic flows [31].

It has been observed that the default HIJING values for the Lund string fragmentation parameters ($a = 0.5$ and $b = 0.9 \text{ GeV}^{-2}$) in set B were able to describe the pp data when used in the AMPT default model but underestimated the charged particle yield in central Pb + Pb collisions at the top Super Proton Synchrotron (SPS) energy [38–40]. For Pb+Pb collisions at Large Hadron Collider (LHC) energies, the AMPT SM model with default HIJING values for the Lund string fragmentation parameters ($a = 0.5$ and $b = 0.9 \text{ GeV}^{-2}$) in set B was able to reproduce the yield and elliptic flow of charged particles but underestimated the p_T spectrum except at low p_T [31, 38].

From Eq. (2) it is clear that parameters a and b determine the p_T distribution of the particles. For larger a and b there will be a smaller average square transverse momentum that will produce a steeper p_T spectrum (with large slope), while their smaller values will lead to a flatter distribution. It has been reported that the values of $a = 2.2$ and $b = 0.5 \text{ GeV}^{-2}$ produce larger multiplicity density as compared to other values of a and b [31]. Thus, the modified values of $a = 2.2$ and $b = 0.5 \text{ GeV}^{-2}$ (set C) were used to fit the charged particle yield in Pb+Pb collisions at SPS [38, 40]. For heavy-ion collisions at RHIC energies, the default AMPT model with these parameters was found to reasonably fit the rapidity and pseudorapidity density and the p_T spectra but underestimate the elliptic flow [38, 40]. On using the AMPT SM with same parameters, the elliptic flow and two-pion Hanbury

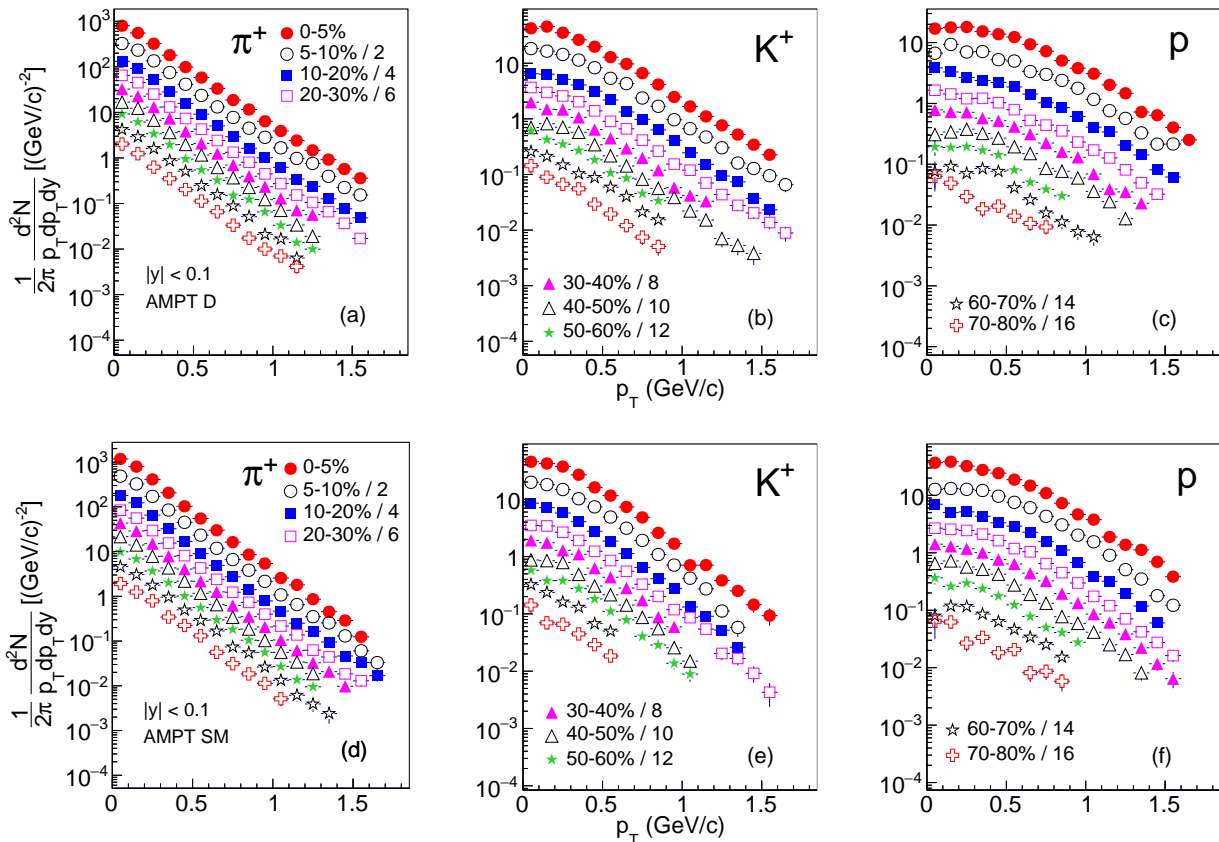


FIG. 1: Midrapidity ($|y| < 0.1$) transverse momentum spectra of π^+ , K^+ , p in Au + Au collisions at $\sqrt{s_{NN}} = 27$ GeV at different centralities using set B (HIJING default $a = 0.5$, $b = 0.9$ GeV^{-2} , and $\sigma = 1.5\text{mb}$) parameters in default [(a)–(c)] and string melting [(d)–(f)] versions of the AMPT model. Spectra for centralities other than 0-5% are scaled for clarity as shown in figure.

Brown and Twiss correlations (HBT) were reproduced but the charged particle yield was overestimated while the slopes of the p_T spectra were underestimated [28, 38].

In order to simultaneously fit the rapidity density, p_T spectrum, and elliptic flow of pions and kaons at low p_T in Au+Au collisions at RHIC energies, the AMPT SM model was used with modified Lund string fragmentation parameters $a = 0.55$ and $b = 0.15$ GeV^{-2} in set A [38].

Thus we observe that each of these sets satisfactorily describes the heavy-ion data at different energies from various experiments. The availability of centrality dependent results at the RHIC for a vast range of energies allows us to test the validity of the given parameters at these conditions. We have generated AMPT events for Au+Au collisions at three energies, viz., the lowest RHIC energy (7.7 GeV), an intermediate energy (27 GeV), and the top RHIC energy of 200 GeV. The model version `ampt-v1.26t7-v2.26t7` is used for this study. The events are generated using both string melting and default versions of the AMPT. For each of these versions, we have used the three sets of parameters listed in Table I to generate the events. About 20000 events are used for the

analysis at each energy, for each set, and for each of the two versions of the model. The centrality selection is done in the same way as in the experimental data [18]. Thus, the AMPT data are divided into nine centrality classes: 0-5%, 5-10%, 10-20%, 20-30%, 30-40%, 40-50%, 50-60%, 60-70%, and 70-80%.

III. RESULTS

We present the mid-rapidity ($|y| < 0.1$) transverse momentum p_T spectra, particle yields dN/dy , average transverse momentum $\langle p_T \rangle$ and ratios of identified particles π^\pm , K^\pm , p , and \bar{p} at $\sqrt{s_{NN}} = 7.7$, 27, and 200 GeV. The results are obtained for both AMPT SM and default versions at each energy and using three different sets of parameters listed in Table I. The simulated results are compared with corresponding results from the STAR experiment.

A. Transverse momentum spectra

Figure 1 shows the invariant yield versus p_T in Au+Au collisions at $\sqrt{s_{NN}} = 27$ GeV for positively charged particles (π^+ , K^+ , p). The results are shown using the set B parameters for representation. The top three panels [(a)–(c)] represent the results for the default AMPT version while the AMPT string melting results are shown in the bottom three panels [(d)–(f)]. Results from the nine collision centralities 0-5%, 5-10%, 10-20%, 20-30%, 30-40%, 40-50%, 60-70%, and 70-80% are shown. The invariant yield decreases with increasing p_T and also while going from central to peripheral collisions. On comparing the inverse slopes of the spectra for three particles, we observe that they follow the order $p > K > \pi$. The same behavior is observed at 7.7 and 200 GeV and for all parameter sets. The negatively charged particles (not presented here) also show similar behavior.

Figure 2 compares the p_T spectra of π^+ , K^+ , and p for both versions of the AMPT model and using the three different parameter sets with experimental data in Au+Au collisions at $\sqrt{s_{NN}} = 7.7$ and 200 GeV for 0–5% collision centrality. The top six panels [(a)–(f)] represent the comparison of default model with the experimental data, while the six panels at the bottom [(g)–(l)] represent the same for the string melting version. The data-to-model ratios are shown at the bottom of each plot. For the default version, at 7.7 GeV, set B parameters describe the π^+ spectra better. Both the K^+ and p spectra are described better by the set A parameters at this energy. At 27 GeV (plots not presented here), the π^+ spectra is described well by set C parameters. The K^+ and p spectra are explained better by set A parameters. At 200 GeV, the set A and B parameters describe the π^+ and K^+ while set A describes the p spectra better as compared to the other sets.

For string melting, at 7.7, 27 (plots not presented here), and 200 GeV, set A parameters describe the π^+ and p spectra well for 0–5% centrality. The K^+ spectra at 7.7 GeV are underpredicted by all sets by about a factor of 2, with set A parameters showing a better p_T dependence. At 27 GeV, the data-to-model ratio comes closer to unity for set A parameters but is still underpredicted. At 200 GeV, the ratio of data to model for K^+ becomes less than unity. Thus, the ratio of data to model for K^+ decreases with increasing energy from about 2 at 7.7 GeV to just less than unity at 200 GeV using set A parameters. This suggests that the string melting version is important for description of kaons towards higher center-of-mass collision energies but does not characterize lower energy collisions well.

To summarize the observations from Fig. 2:

- *The pion spectrum at 7.7 GeV is described well by SM model set A parameters. At 27 GeV, it is described better by default set A parameters. At 200 GeV, it is described by both default and SM set A parameters.*

- *The kaon spectra at 7.7 and 27 GeV are described better by default set A parameters. At 200 GeV, they are described adequately by default set A parameters but are slightly overestimated.*
- *The proton spectra at 7.7 and 27 GeV are described well by SM set A parameters at low p_T and by default set A parameters at high p_T . At 200 GeV, the spectra are described adequately by both default and SM set A parameters.*

The spectra comparison are quantified by comparing particle yields, average transverse momenta, and particle ratios.

B. Particle yields (dN/dy)

Figure 3 shows the centrality dependence of yield dN/dy normalized by half the number of participants, $\langle N_{\text{part}} \rangle / 2$, for π^+ , K^+ , and protons in Au+Au collisions at 7.7, 27, and 200 GeV. The results from the default version are shown in the top three rows [(a)–(i)], while those using the string melting version are shown in the bottom three rows [(j)–(r)]. The results using the three sets of parameters in both the model versions are compared with the experimental data. The experimental data show an increase of yield from peripheral to central collisions suggesting particle production by both soft and hard processes.

In the default version, the $(dN/dy)/(0.5\langle N_{\text{part}} \rangle)$ of π^+ at 7.7 GeV is described by set B parameters at all $\langle N_{\text{part}} \rangle$ values. At 27 GeV, set C parameters agree with data at all $\langle N_{\text{part}} \rangle$ values, but $\langle N_{\text{part}} \rangle$ dependence is flat as opposed to the data in which it increases from peripheral to central collisions. At 200 GeV, none of the sets could explain the behavior observed in data for all $\langle N_{\text{part}} \rangle$ values. The set A parameters could only describe the data for $\langle N_{\text{part}} \rangle > 100$ while set C parameters agree with data for $\langle N_{\text{part}} \rangle < 40$. The K^+ yields at 7.7 GeV are not explained by any of the parameter sets for all $\langle N_{\text{part}} \rangle$. The set A parameters can only describe the data for $\langle N_{\text{part}} \rangle < 120$. At 27 GeV, K^+ yields are better described by set C parameters for all $\langle N_{\text{part}} \rangle$, while at 200 GeV, the set A parameters describe the K^+ yields for all $\langle N_{\text{part}} \rangle$. The proton yields are described by all the parameter sets at all $\langle N_{\text{part}} \rangle$ for 7.7 GeV, but none of them work for 27 GeV other than sets A and C at $\langle N_{\text{part}} \rangle < 30$, whereas at 200 GeV none of the parameters could explain the p yields at any centrality.

For the AMPT model with string melting, the $(dN/dy)/(0.5\langle N_{\text{part}} \rangle)$ of π^+ at 7.7 GeV is described by all the parameters at all N_{part} values. However, the set C parameters show a rather flat behavior as opposed to the slight increase from peripheral to central collisions. At 27 GeV, the set C parameters describe the π^+ yields at all $\langle N_{\text{part}} \rangle$ values but set A and B parameters are closer in agreement with the data in peripheral collisions. At 200 GeV, in central collisions ($\langle N_{\text{part}} \rangle > 100$), pion yields

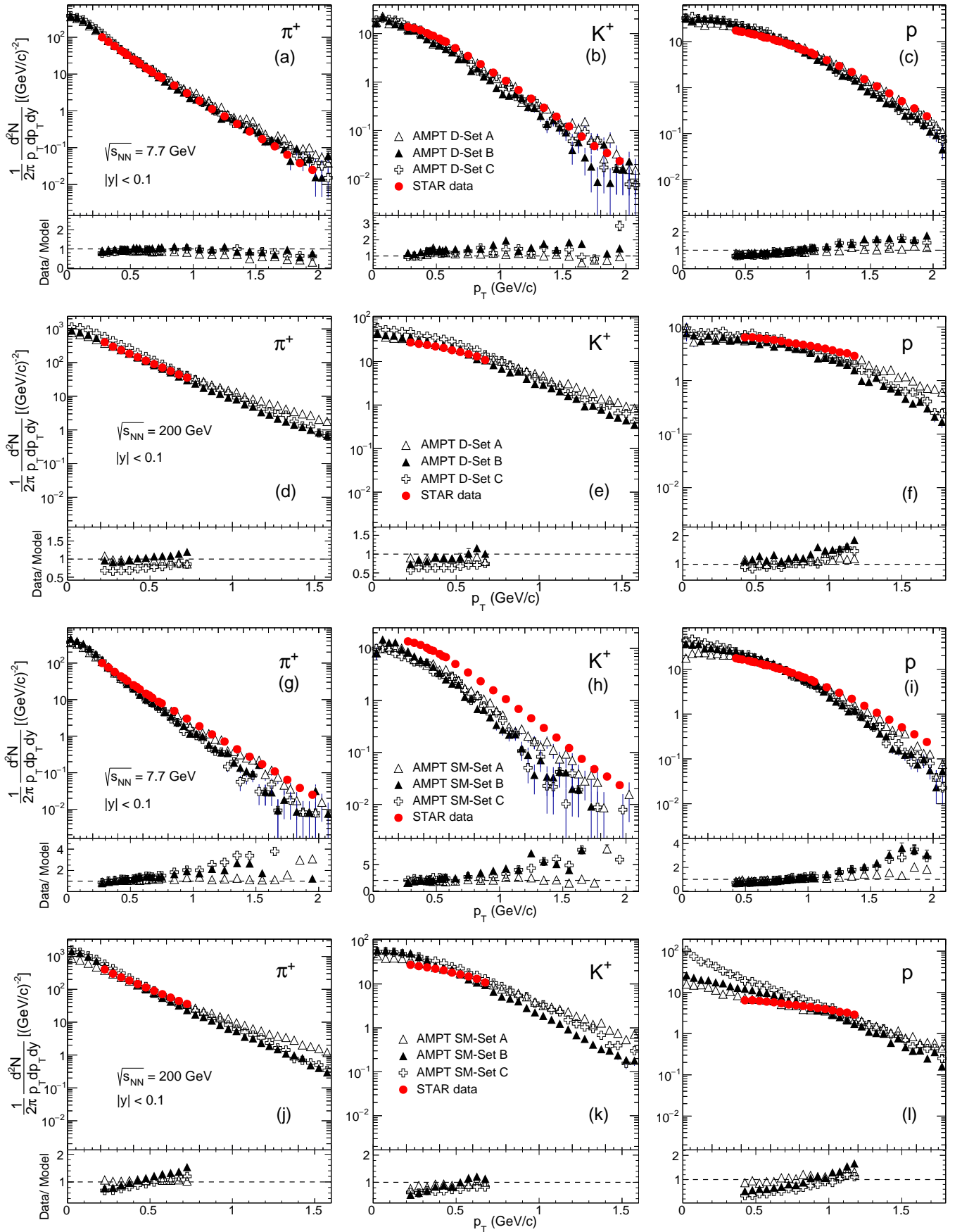


FIG. 2: Midrapidity ($|y| < 0.1$) transverse momentum spectra of π^+ , K^+ , p at $\sqrt{s_{NN}} = 7.7$ and 200 GeV for 0-5% central Au + Au collisions from default [(a)–(f)] and string melting [(g)–(l)] versions of the AMPT model using parameter sets A, B, and C. Experimental data from the STAR Collaboration [18, 41] are shown by solid circles. The data-to-model ratios are presented at the bottom of each panel.

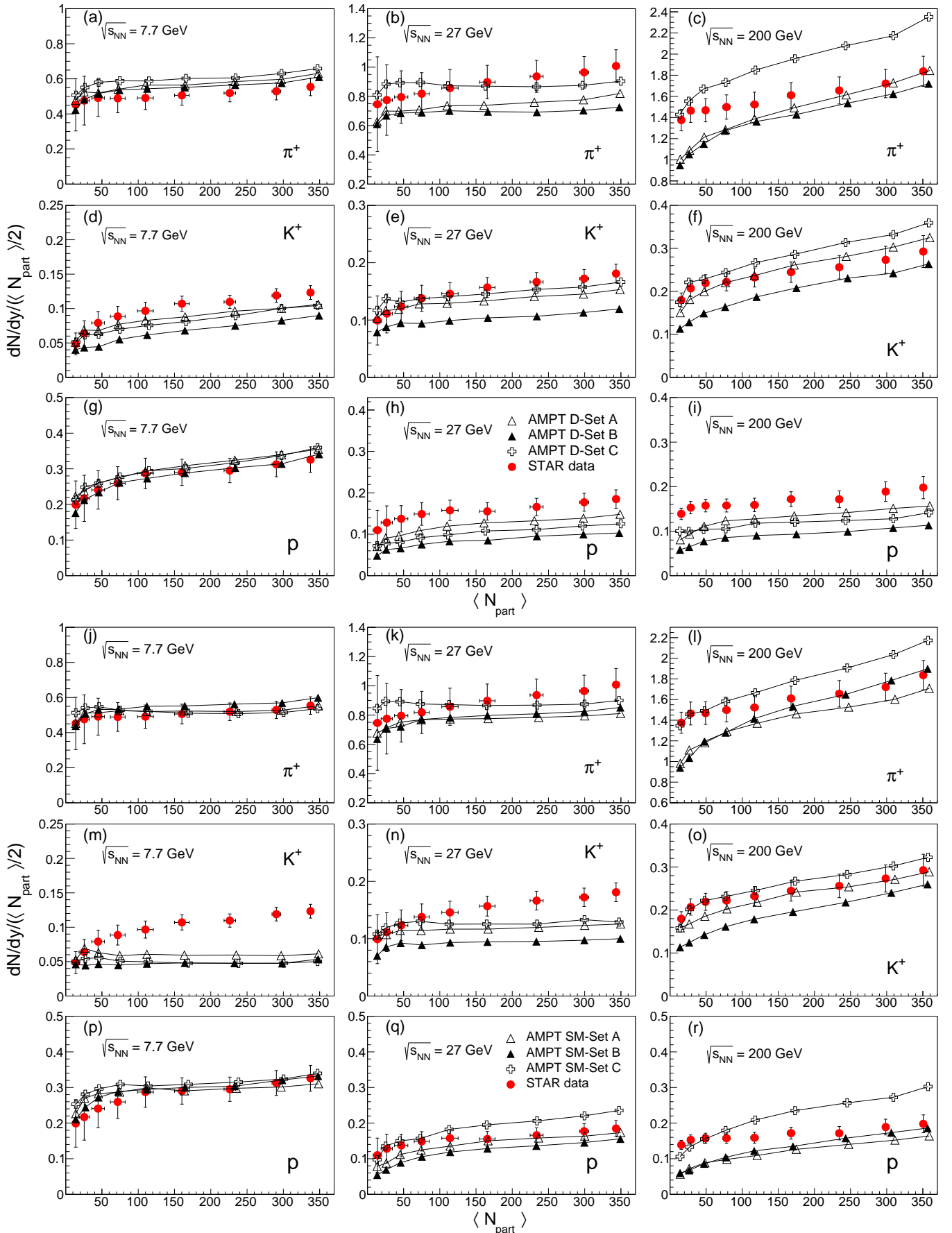


FIG. 3: Centrality dependence of dN/dy normalized by half participant $\langle N_{\text{part}} \rangle / 2$ for positive particles at mid-rapidity ($|y| < 0.1$) in Au+Au collisions at $\sqrt{s_{\text{NN}}} = 7.7, 27, 200$ GeV from the AMPT default [(a)–(i)] and string melting [(j)–(r)] models. Results are presented using the parameter sets A, B, and C. Experimental data from the STAR Collaboration[18, 41] are shown by solid circles.

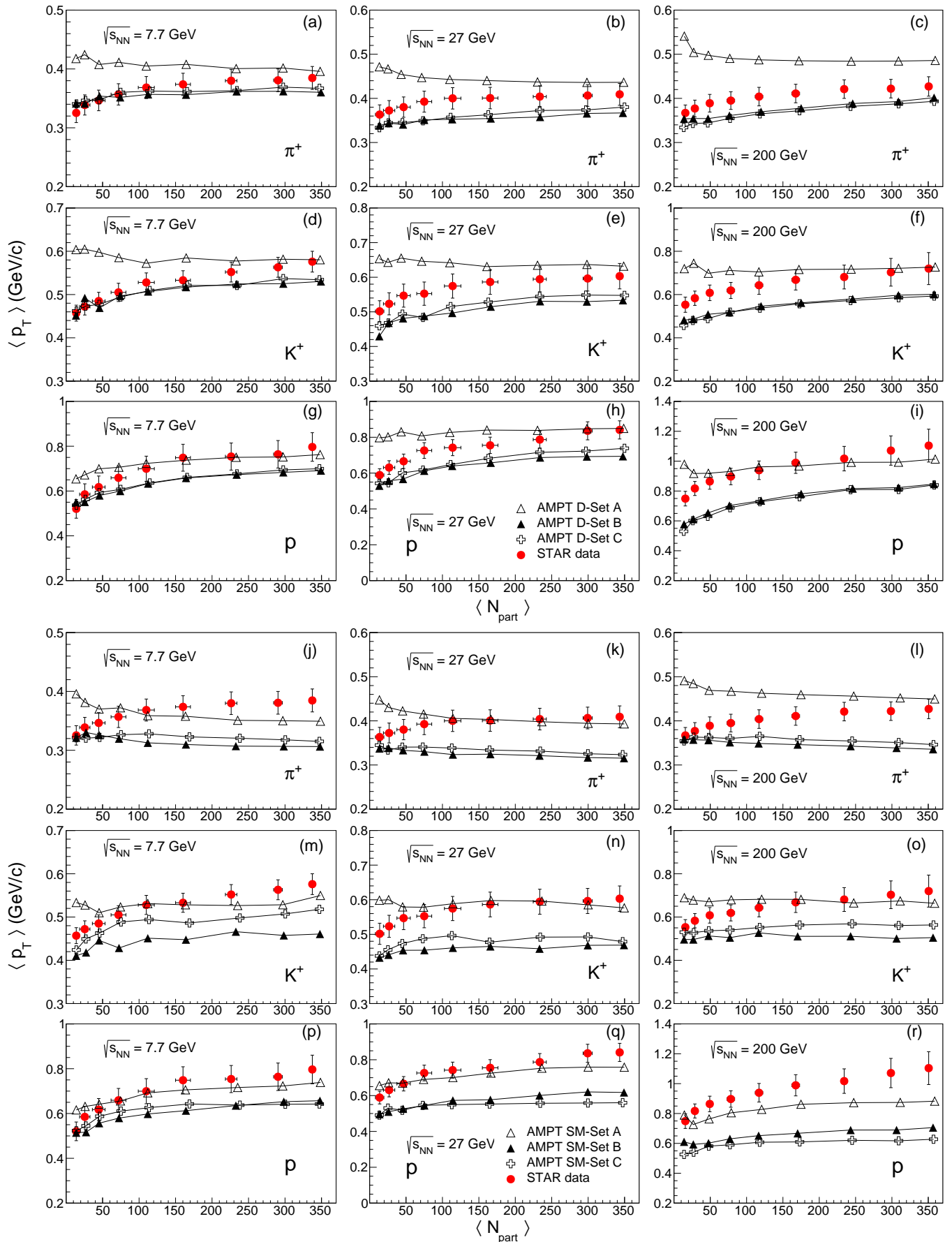


FIG. 4: Centrality dependence of $\langle p_T \rangle$ for positive particles at mid-rapidity ($|y| < 0.1$) in Au+Au collisions at $\sqrt{s_{NN}} = 7.7, 27,$ and 200 GeV from the AMPT default [(a)–(i)] and string melting [(j)–(r)] models. Results are presented using the parameter sets A,B, and C. Experimental data from the STAR Collaboration[18, 41] are shown by solid circles.

are well described by set B parameters while those in peripheral collisions ($\langle N_{\text{part}} \rangle < 130$) are described by set C parameters. The K^+ yields are only described by set A parameters below $\langle N_{\text{part}} \rangle 50$ at 7.7 GeV, below $\langle N_{\text{part}} \rangle 130$ by set C parameters at 27 GeV, and for all $\langle N_{\text{part}} \rangle$ by set C parameters at 200 GeV. The proton yields at 7.7 GeV are described by all parameter sets at all $\langle N_{\text{part}} \rangle$, at 27 GeV by set A parameters at all $\langle N_{\text{part}} \rangle$, and at 200 GeV by set B parameters for $\langle N_{\text{part}} \rangle > 220$ and by set C parameters for $\langle N_{\text{part}} \rangle < 90$ but not by any parameter set at the most peripheral point.

To summarize the observations for all centralities:

- The pion yield is described by set C parameters for $\sqrt{s_{NN}} \leq 27$ GeV for the SM model, but by none of the models at 200 GeV. However, the 200 GeV pion yield is constrained between sets A and C at all $\langle N_{\text{part}} \rangle$ for both versions of AMPT.
- The kaon yield at 7.7 GeV is not explained at all $\langle N_{\text{part}} \rangle$ by any set with either versions (the models underestimate the data), explained at 27 GeV by the default model with set C parameters and also at 200 GeV by the default model with set A parameters and by the SM model with set C parameters. Thus, at 7.7 GeV, the kaon (strange particle) production is not explained by the AMPT model.
- The proton yield at 7.7 GeV is explained by all parameter sets with both the models, at 27 GeV by set A parameters with the SM model, but by none of the models at 200 GeV. However, the 200 GeV proton yield is constrained between sets B and C at all $\langle N_{\text{part}} \rangle$ for the AMPT SM version.
- In general, for most cases, it is observed that the set C parameters corresponding to largest $a = 2.2$ give higher yields while set B parameters corresponding to the smallest $a = 0.5$ give smaller yields, as expected.

C. Average transverse momentum ($\langle p_T \rangle$)

Figure 4 shows the centrality dependence of average transverse momentum $\langle p_T \rangle$ for π^+ , K^+ , and protons in Au+Au collisions at $\sqrt{s_{NN}} = 7.7, 27,$ and 200 GeV. The results from the default version are shown in the top three rows [(a)–(i)] while those from the string melting version are shown in the bottom three rows [(j)–(r)]. The results using the three parameter sets A, B, and C are compared with experimental data using both the default and string melting versions. The data show increase of $\langle p_T \rangle$ from peripheral to central collisions suggesting increasing radial flow towards central collisions. The $\langle p_T \rangle$ reflects the shape (slope) of the spectra.

Using the default version, $\langle p_T \rangle$ of π^+ at 7.7 GeV is described by set C parameters for all $\langle N_{\text{part}} \rangle$. At 27 GeV, set A and set C parameters agree with data at $\langle N_{\text{part}} \rangle >$

220. While the set A parameters do not follow the behavior of data, set B and C reproduce the data qualitatively and tend to agree with them at the last two peripheral points. At 200 GeV, none of the sets could explain the behavior observed in data for all $\langle N_{\text{part}} \rangle$ values. The set B parameters only describe the most peripheral data. The K^+ $\langle p_T \rangle$ at 7.7 GeV can only be explained by set A parameters for $\langle N_{\text{part}} \rangle > 220$, and by sets B and C for $\langle N_{\text{part}} \rangle < 170$. At 27 GeV, K^+ $\langle p_T \rangle$ are better described by set A parameters for $\langle N_{\text{part}} \rangle > 150$. Set A shows a flat behavior with $\langle N_{\text{part}} \rangle$. However, sets B and C only qualitatively describe the experimental data. At 200 GeV, set A parameters describe the K^+ $\langle p_T \rangle$ for $\langle N_{\text{part}} \rangle > 150$. Both set B and C parameters underestimate the data at all $\langle N_{\text{part}} \rangle$. For protons at 7.7 GeV, $\langle p_T \rangle$ are described by set A parameters for $\langle N_{\text{part}} \rangle > 50$ and by both sets B and C below $\langle N_{\text{part}} \rangle \approx 80$. At 27 GeV, set A parameters describe the protons' $\langle p_T \rangle$ for $\langle N_{\text{part}} \rangle > 220$. For peripheral collisions, set B and C parameters give closer $\langle p_T \rangle$ values to experimental data but underestimate nevertheless. At 200 GeV, the set A parameters could explain the p $\langle p_T \rangle$ for all $\langle N_{\text{part}} \rangle$ values except the two peripheral bins. The other two parameter sets underestimated the data quite significantly.

For AMPT string melting, the $\langle p_T \rangle$ of π^+ at 7.7 GeV is described by set A parameters at three mid-central collisions but is underestimated (overestimated) at central (peripheral) collisions. Sets B and C can only describe the data at the last three peripheral bins. At 27 GeV, the set A parameters could explain the data for $\langle N_{\text{part}} \rangle \geq 70$ while set B and C parameters could only agree with data at the most peripheral bin. Increasing the energy further to 200 GeV leads to the overestimation of data by set A parameters with only the most central point being sufficiently close to the data. Set C can describe the data at the three most peripheral points and set B at the two most peripheral points. The K^+ $\langle p_T \rangle$ at 7.7 GeV are described by set A parameters for four mid-central points but are underestimated (overestimated) at central (peripheral) collisions. The set C parameters tend to describe the data for $\langle N_{\text{part}} \rangle < 90$. Increasing the energy to 27 GeV, for K^+ , leads to better agreement also in central collisions by set A parameters. These parameters describe the data for all but the last two most peripheral $\langle N_{\text{part}} \rangle$ values. Increasing the energy further to 200 GeV, for K^+ , does not change the results much for set A parameters which still describe the data from mid-central to central collisions. Using set C parameters for K^+ , the model agrees with data at the most peripheral point. The proton $\langle p_T \rangle$ at 7.7 GeV are described by set A parameters at all $\langle N_{\text{part}} \rangle$ except at the most peripheral bin. The set C parameters seem to describe the data at peripheral collisions below $\langle N_{\text{part}} \rangle \approx 100$. At 27 GeV, the set A parameters describe the proton data at all but the two most central points and the most peripheral point. The other two parameter sets underestimate the data. At 200 GeV, the set A parameters only describe the proton data at most peripheral bin and underestimate the data for

all other $\langle N_{\text{part}} \rangle$ values. The sets B and C underestimate the data at all $\langle N_{\text{part}} \rangle$ values.

To summarize the above observations:

- The $\langle p_{\text{T}} \rangle$ of pions at 7.7 GeV is described at all $\langle N_{\text{part}} \rangle$ by default AMPT set C parameters. At 27 GeV, it is described by AMPT SM set A parameters for only $\langle N_{\text{part}} \rangle > 50$ and is constrained between sets A and C below that. At 200 GeV, it is explained by none of the models but constrained between sets A and B for both the default and SM versions.
- The $\langle p_{\text{T}} \rangle$ of kaons at 7.7 GeV is described partially by default AMPT set A parameters for $\langle N_{\text{part}} \rangle > 220$, and by default AMPT set B and C parameters for $\langle N_{\text{part}} \rangle < 170$. At 27 GeV, it is explained by SM set A parameters for all $\langle N_{\text{part}} \rangle$ except at the two most peripheral points. For the two most peripheral bins, it is constrained between SM sets A and C. At 200 GeV, it is explained by default and SM set A parameters for $\langle N_{\text{part}} \rangle > 100$. Below that, it is constrained better between SM sets A and C.
- The proton $\langle p_{\text{T}} \rangle$ at 7.7 GeV is described by SM set A parameters at all $\langle N_{\text{part}} \rangle$ except the most peripheral bin. The SM sets B and C describe the peripheral bin. At 27 GeV, again, SM set A parameters work better for all but the most peripheral bin and two most central bins. At 200 GeV, the proton $\langle p_{\text{T}} \rangle$ is explained at all but last two peripheral bins by default set A parameters. The last two bins are constrained between default sets A and B.

D. Particle ratios

In Fig. 5, we show the centrality dependence of various antiparticle-to-particle (π^-/π^+ , K^-/K^+ , \bar{p}/p) ratios at mid-rapidity ($|y| < 0.1$) in Au+Au collisions at $\sqrt{s_{\text{NN}}} = 7.7, 27,$ and 200 GeV obtained from the default [(a)–(i)] and SM [(j)–(r)] AMPT models using the three parameter sets A, B, and C. The results are again compared with the corresponding experimental data.

The default AMPT model could reasonably predict the π^-/π^+ ratio at the three energies with all the parameter cases. The K^-/K^+ ratio at 7.7 GeV is mostly underestimated by set A parameters while the set B and set C parameters give closer values to data in general. At 27 GeV, the results with the three parameter sets are close to each other and the data, agreeing marginally with the data. At 200 GeV, the K^-/K^+ ratio is mostly underestimated by three parameter sets but matches with the data in peripheral collisions. The \bar{p}/p ratio at 7.7 GeV is mostly overestimated by all the three parameter sets. For $\langle N_{\text{part}} \rangle < 90$ (except the most peripheral bin), set B parameters explain the data. At 27 GeV, the \bar{p}/p ratio is explained by set B parameters for $\langle N_{\text{part}} \rangle > 100$. At 200 GeV, all the three parameter sets seem to describe

the \bar{p}/p ratio, with the exception of the most peripheral point by set A parameters.

Similar to the default model, the AMPT model with string melting could reasonably predict the π^-/π^+ ratio at the three energies with all the three parameter cases. The K^-/K^+ ratio at 7.7 GeV is generally described by set C parameters for central collisions $\langle N_{\text{part}} \rangle > 150$. Set B parameters could only explain the ratio at three points before the most peripheral bin. At 27 and 200 GeV, set A parameters describe the data at all centralities. The set B parameters could also explain the data at all but two centralities. The \bar{p}/p ratio at 7.7 GeV is described by the set C parameters for all centralities except at the two most peripheral bins. At 27 GeV, it is described by the set C parameters at all centralities. At 200 GeV, all three sets give similar values, close to the experimental \bar{p}/p ratio.

The mixed particle ratio results could help in better differentiating among the three parameter sets. In Fig. 6, we show the centrality dependence of various mixed (K^+/π^+ , K^-/π^- , p/π^+ , \bar{p}/π^-) particle ratios at mid-rapidity ($|y| < 0.1$) in Au+Au collisions at $\sqrt{s_{\text{NN}}} = 7.7, 27,$ and 200 GeV obtained from the default [(a)–(l)] and SM [(m)–(x)] AMPT models using the three parameter sets A, B, and C. The results are compared with the corresponding experimental data.

For default AMPT model, the K^+/π^+ ratio at 7.7 GeV is not explained by any of the parameter sets except at very peripheral collisions. At 27 GeV, the K^+/π^+ ratio is described by set C parameters at all $\langle N_{\text{part}} \rangle$. The set A parameters describe the data at all centralities except at the most peripheral one, while set B parameters describe the ratio at almost all $\langle N_{\text{part}} \rangle$ values except in mid-central collisions. Similar conclusions could be drawn for 200 GeV except that the set A parameters now miss the data at more $\langle N_{\text{part}} \rangle$ values. The same as the K^+/π^+ ratio, the K^-/π^- ratio at 7.7 GeV is also not described by any of the three parameter sets except at the very peripheral points. At 27 GeV, the ratio is well explained by set C parameters for all $\langle N_{\text{part}} \rangle$. The set A parameters also describe the data at all $\langle N_{\text{part}} \rangle$ except at the most peripheral bin, while set C parameters work well at peripheral collisions. Similar conclusions could be drawn at 200 GeV except that the set C parameters also miss a few points towards the peripheral collisions. Thus, in this case, set A describes the data better at all $\langle N_{\text{part}} \rangle$ except the peripheral point. The p/π^+ ratio at 7.7 GeV is described by all parameter sets at all $\langle N_{\text{part}} \rangle$. At 27 GeV, the ratio is described by set A parameters at all $\langle N_{\text{part}} \rangle$. At 200 GeV, the p/π^+ ratio predicted by set A parameters is closer to data but does not agree exactly with it. The \bar{p}/π^- ratio at 7.7 GeV is described by set B and C parameters at all $\langle N_{\text{part}} \rangle$ except at one bin towards peripheral collisions. At 27 GeV, it is described well by set C parameters at all $\langle N_{\text{part}} \rangle$ values. Set B also describes this ratio at almost all the centralities. At 200 GeV, the ratio is explained by set A parameters for all $\langle N_{\text{part}} \rangle$.

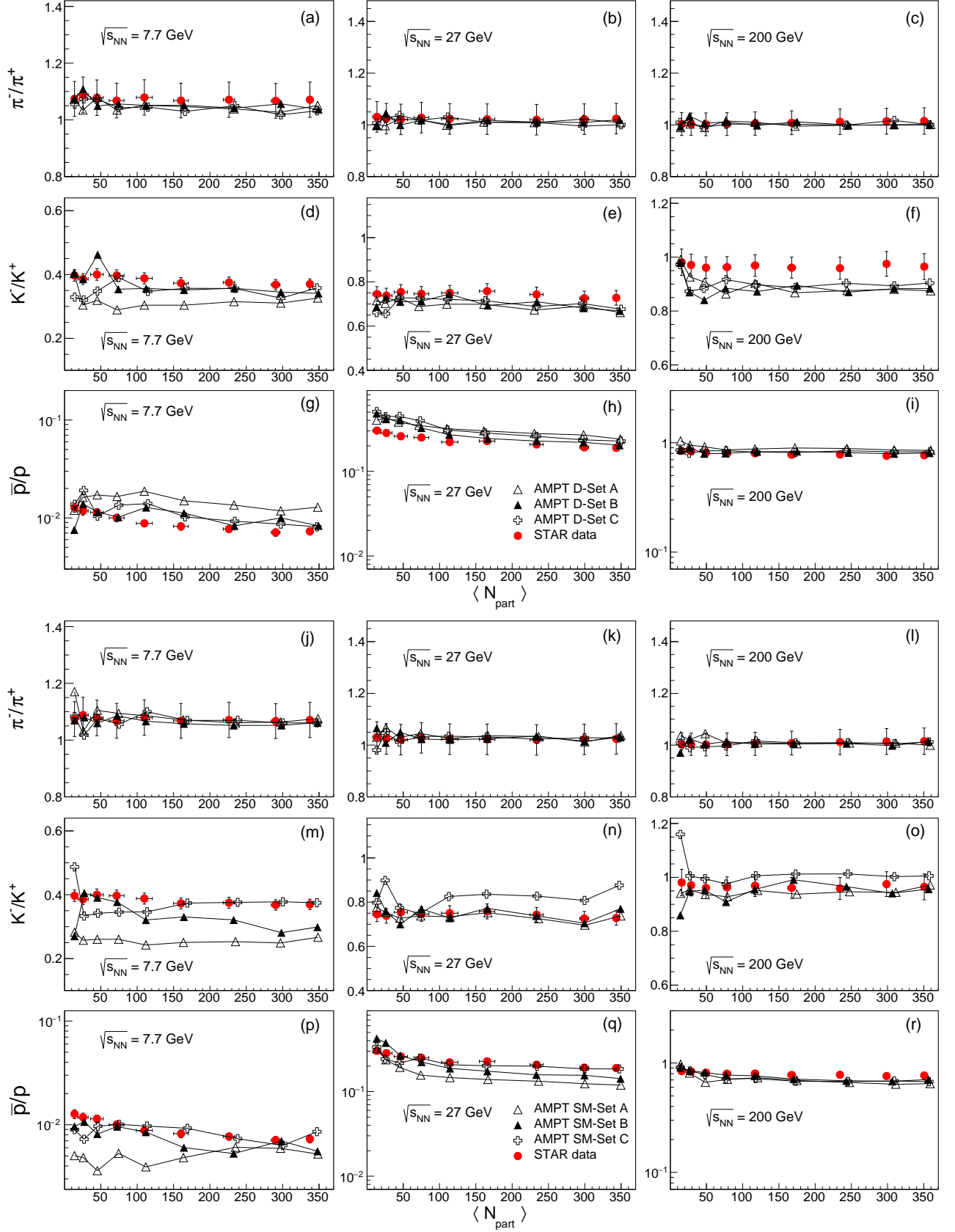


FIG. 5: Centrality dependence of antiparticle-to-particle (π^-/π^+ , K^-/K^+ , \bar{p}/p) ratios at mid-rapidity ($|y| < 0.1$) in Au + Au collisions at $\sqrt{s_{NN}} = 7.7, 27,$ and 200 GeV from the AMPT default [(a)–(i)] and SM [(j)–(r)] models. Results are presented using the parameter sets A, B and C. Experimental data from the STAR Collaboration [18, 41] are shown by solid circles.

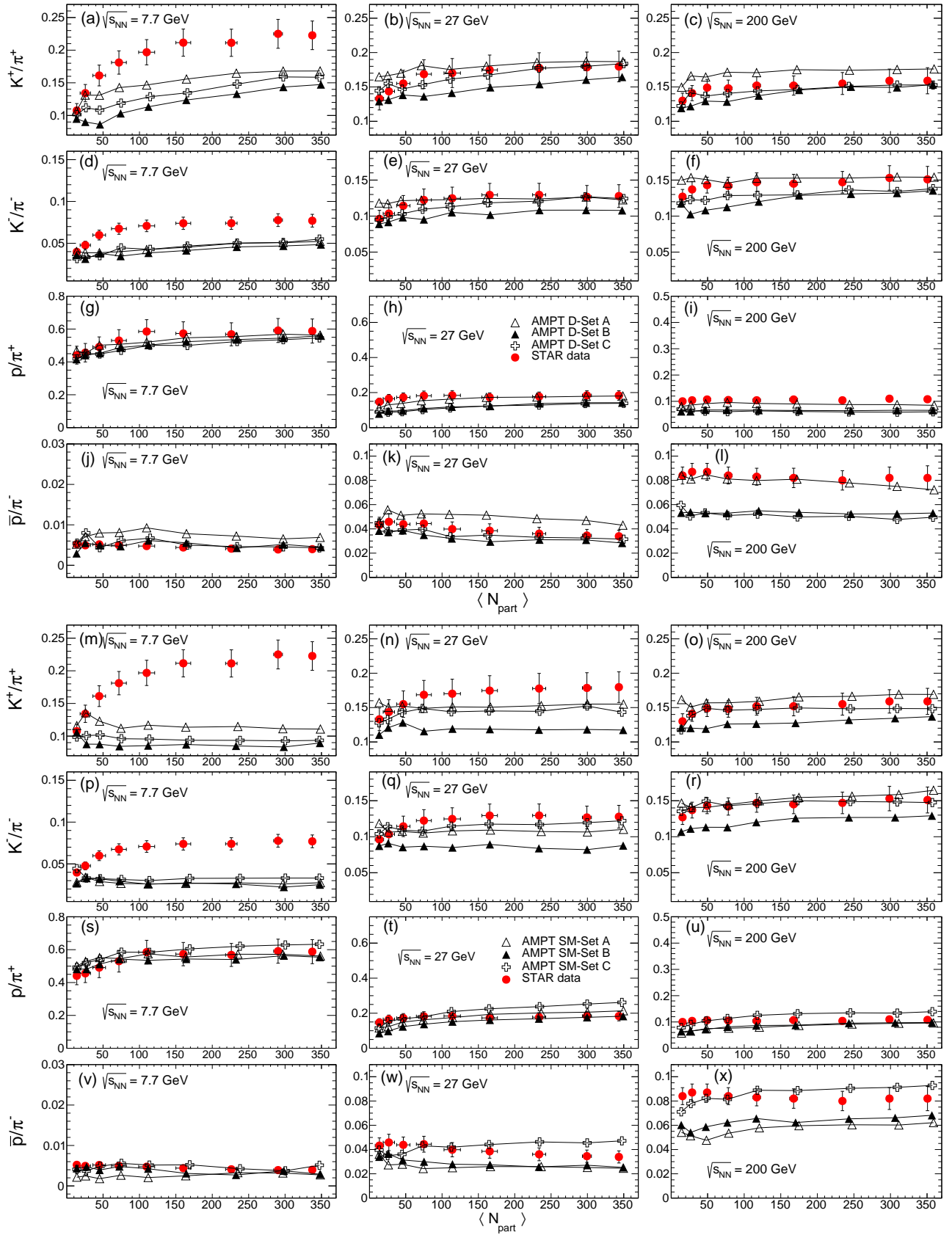


FIG. 6: Centrality dependence of mixed particle (K^+/π^+ , K^-/π^- , p/π^+ , \bar{p}/π^-) ratios at mid-rapidity ($|y| < 0.1$) in Au + Au collisions at $\sqrt{s_{NN}} = 7.7, 27,$ and 200 GeV from the default [(a)–(l)] and AMPT SM [(m)–(x)] models. Results are presented using the parameter sets A, B, and C. Experimental data from the STAR Collaboration [18, 41] are shown by solid circles.

For the AMPT SM model, the K^+/π^+ ratio at 7.7 GeV is not explained by any parameter set except at the most peripheral collision. It is interesting to note that no set shows even the qualitative behavior of centrality dependence observed in experimental data. At 27 GeV, the K^+/π^+ ratio is marginally described by set A parameters for most centralities except the peripheral ones. However, the $\langle N_{\text{part}} \rangle$ dependence is well predicted by set C parameters though they consistently underestimate the data. At 200 GeV, the set C parameters describe the data at all centralities. The set A parameters also describe the K^+/π^+ ratio for all centralities except at the most peripheral collisions. The K^-/π^- ratio at 7.7 GeV is also not described by any of the three parameter sets except at the most peripheral point by set C. At 27 GeV, the ratio is well explained by set C parameters for all $\langle N_{\text{part}} \rangle$. The set A parameters also result in closer values to the data at most centralities. At 200 GeV, set C parameters describe the data at all centralities. Set A also describes the data at all centralities except at the most peripheral bin. The p/π^+ ratio at 7.7 GeV is described by all parameter sets at all $\langle N_{\text{part}} \rangle$. At 27 GeV, the ratio is described by set A parameters at all $\langle N_{\text{part}} \rangle$. The set B parameters describe the data for central collisions but fail at peripheral collisions while the set C parameters describe the data at peripheral collisions failing at central collisions. At 200 GeV, the p/π^+ ratio is described by set A and B parameters towards the central collisions ($\langle N_{\text{part}} \rangle > 200$) and by set C parameters towards peripheral collisions ($\langle N_{\text{part}} \rangle < 150$). The \bar{p}/π^- ratio at 7.7 GeV is described by both set B and C parameters at almost all $\langle N_{\text{part}} \rangle$. At 27 GeV, the ratio is described by set C parameters from mid-central ($\langle N_{\text{part}} \rangle < 200$) to peripheral collisions. At 200 GeV, the ratio is described by set C parameters for most $\langle N_{\text{part}} \rangle$ except at a few centrality bins.

To summarize the observations from the two models (Figs. 5 and 6) :

- The π^-/π^+ ratio is described by both default and SM models using the sets A, B and C at the three energies $\sqrt{s_{NN}} = 7.7, 27, \text{ and } 200 \text{ GeV}$.
- The K^-/K^+ ratio at 7.7 GeV is better described by SM set C parameters for $\langle N_{\text{part}} \rangle > 150$. At 27 and 200 GeV, it is described at all $\langle N_{\text{part}} \rangle$ by SM set A parameters.
- The \bar{p}/p ratio at 7.7 GeV is described better by SM set C parameters for all centralities except at the last two peripheral bins. At 27 GeV, the ratio is described well by SM set C parameters and at 200 GeV by default set B parameters at all centralities.
- The K^+/π^+ ratio at 7.7 GeV is not described well by any of the models at all centralities, except the peripheral bins. The default model gives similar centrality dependence but underpredicts the data. At 27 GeV, this ratio is described better by default set C parameters at all $\langle N_{\text{part}} \rangle$. At 200 GeV,

it is explained by both default and SM set C parameters at all centralities. Thus, at 7.7 GeV, the strange particle production is not well explained by the AMPT model.

- The K^-/π^- ratio results at 7.7 GeV are similar to those of the K^+/π^+ ratio. The ratio is also not explained by any model at all centralities except at the peripheral bins. At 27 GeV, this ratio is described by both default and SM set C parameters. At 200 GeV, it is explained by SM set C parameters.
- The p/π^+ ratio at 7.7 GeV is explained by both default and SM models with all parameter sets. At 27 GeV, the ratio is described by both default and SM set A parameters at all centralities. However, at 200 GeV, it is not explained by a single parameter set in either model at all the centralities. For central collisions, SM set A and B parameters describe the data while for peripheral collisions SM set C parameters work better.
- The \bar{p}/π^- ratio at 7.7 GeV is described at most $\langle N_{\text{part}} \rangle$ by both default and SM set B and C parameters. At 27 GeV, it is described by default set C parameters and is well explained at 200 GeV by default set A parameters at all $\langle N_{\text{part}} \rangle$.

E. Energy dependence of particle ratios

The particle yields and ratios are used in statistical thermal models to determine the freeze-out conditions in heavy-ion collisions [8–10, 18]. We present the energy dependence of mixed particle ratios for 0–5% central collisions that play an important role in determining the freeze-out conditions.

Figure 7 presents the comparison of K^\pm/π^\pm ratios at mid-rapidity ($|y| < 0.1$) for 0–5% centrality in Au + Au collisions at $\sqrt{s_{NN}} = 7.7, 27, \text{ and } 200 \text{ GeV}$ from the AMPT default [(a),(c)] and SM [(b),(d)] models with experimental data [13, 18, 41–48]. The results from AMPT are presented with the parameters sets A, B, and C. The experimental results of the K^+/π^+ ratio show an interesting trend. The ratio increases with energy, reaches a maximum, and then decreases and becomes almost constant at higher energies. It has been suggested that the peak position, also called the ‘‘horn,’’ in this energy dependence could be a signature of phase transition from hadronic to QGP gas [18, 48]. However, the peak position also corresponds to the energy region with maximum baryon density [49]. For the default AMPT model, the three sets are consistent with data at 27 and 200 GeV. At 7.7 GeV, all the three sets under-predict the ratio significantly. However, among the three sets, the set A parameters are closest to the data. For SM, set A seems to be in better agreement with the data at 27 and 200 GeV but underpredicts the data at 7.7 GeV. Comparing

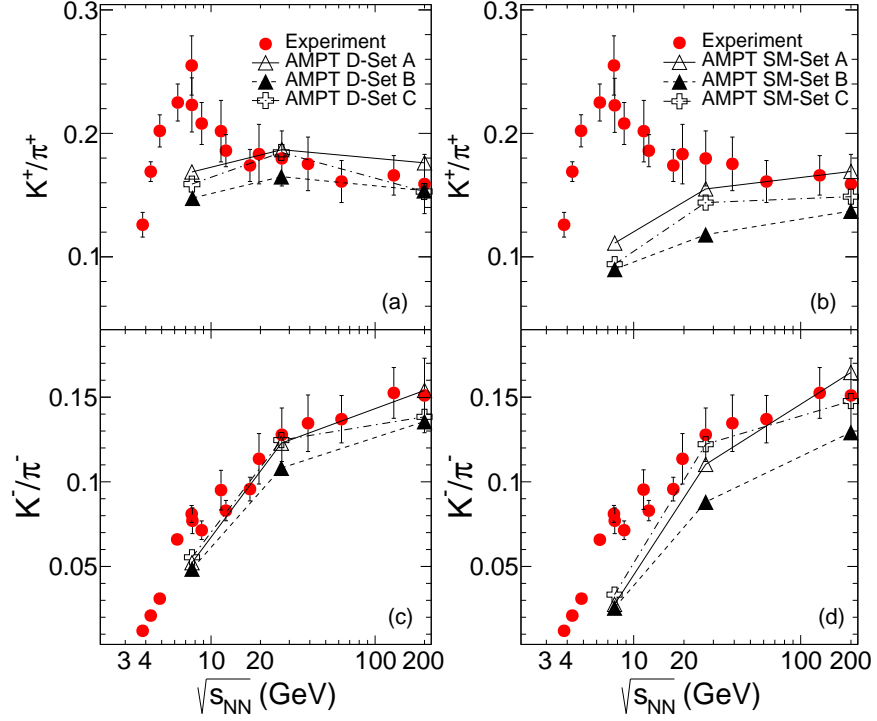


FIG. 7: Comparison of K^\pm/π^\pm ratios at mid-rapidity ($|y| < 0.1$) for 0–5% centrality in Au + Au collisions at $\sqrt{s_{NN}} = 7.7, 27,$ and 200 GeV from the AMPT default [(a),(c)] and SM [(b),(d)] models with experimental data [13, 18, 41–48]. The results from the AMPT model with parameter sets A, B, and C are presented.

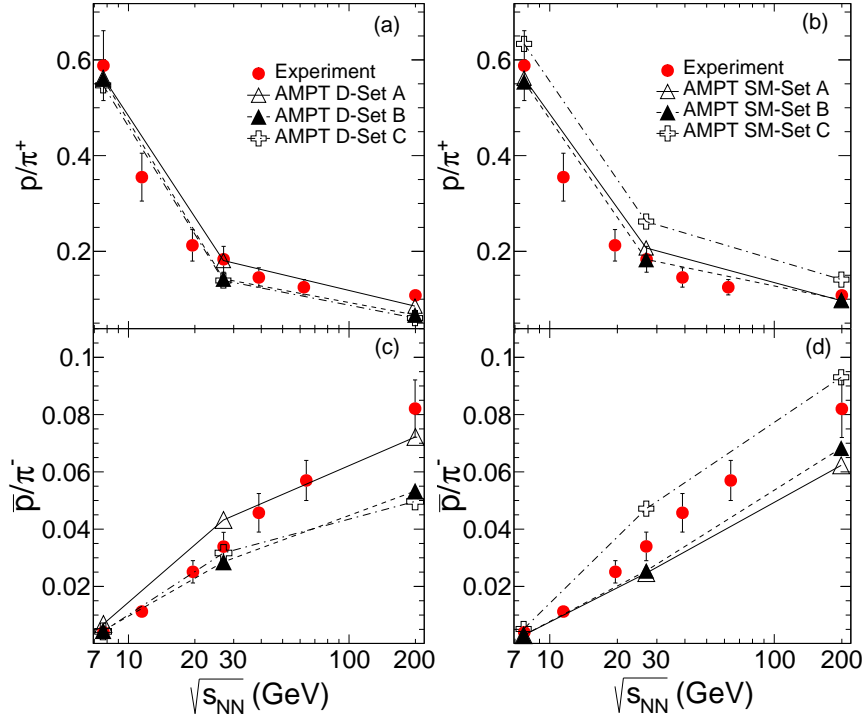


FIG. 8: Comparison of p/π^+ and \bar{p}/π^- ratios at mid-rapidity ($|y| < 0.1$) for 0–5% centrality in Au + Au collisions at $\sqrt{s_{NN}} = 7.7, 27,$ and 200 GeV from the AMPT default [(a),(c)] and SM [(b),(d)] models with experimental data [18, 41]. The results from the AMPT model with parameter sets A, B, and C are presented.

between default and SM, the default set A parameters describe the energy dependence of the K^+/π^+ ratio better. The K^-/π^- ratio at 200 GeV is described by all the three sets of the default and SM models. At 27 GeV, the set A and C parameters are consistent with the data. At 7.7 GeV, the ratio is again underpredicted by both versions. The default model is in closer agreement with data at lower energies. Thus, it can be concluded that strangeness (kaon) production at $\sqrt{s_{NN}} = 7.7$ GeV is not explained by the AMPT model.

Figure 8 shows the comparison of p/π^+ and \bar{p}/π^- ratios at mid-rapidity ($|y| < 0.1$) for 0–5% centrality in Au + Au collisions at $\sqrt{s_{NN}} = 7.7, 27, \text{ and } 200$ GeV from the AMPT default [(a),(c)] and SM [(b),(d)] models with experimental data [18, 41]. The results for AMPT are presented for the parameters sets A, B, and C. In the default model, the set A parameters seem to describe the p/π^+ ratio better at the three energies. With the SM model, both sets A and B describe the data at the three energies. The default AMPT set A parameters describe the \bar{p}/π^- ratio at 7.7 and 200 GeV, while set B and C parameters describe it at 7.7 and 27 GeV. Overall, the set A parameters are closest to the data. For the SM model, the set C parameters describe the ratio at 7.7 and 200 GeV, while sets B and C only describe the data at 7.7 GeV. Again, we observe that the default AMPT model with set A parameters works better than SM model.

In general, considering the energy dependence behavior in 0–5% central Au + Au collisions, we observe that for all observables including yields, $\langle p_T \rangle$ and ratios, the AMPT default model with set A parameters explain the data better than the other sets and also better than AMPT SM with all the sets. However, in recent studies it has been shown that the effect of finite nuclear thickness of incoming colliding nuclei is important at lower energies [50, 51]. So, incorporating the finite nuclear thickness of the incoming colliding nuclei into the AMPT SM model might lead to improvement in the results at lower energies [50].

IV. SUMMARY AND DISCUSSION

This study is an attempt to make the first detailed comparison of light hadron production from the AMPT model with experimental data for three different energies at RHIC, at different centralities and for various identified particles. The default and SM AMPT models were initiated with different sets of parameters (as given in Table I) and the results obtained were compared with the data from the STAR experiment. For this study, we have looked at the bulk properties like transverse momentum spectra, yields, average transverse momentum, and various ratios corresponding to $\pi^\pm, K^\pm, p,$ and \bar{p} . Table II gives a summary of the performance of various sets in AMPT default and SM models for different observables presented. This study also complements the v_2 comparison from AMPT with experimental data previously pub-

lished at these energies.

The spectra comparisons in 0–5% central collisions suggest that set A, corresponding to 3 mb parton cross-section with $a = 0.55$ and $b = 0.15 \text{ GeV}^{-2}$ as Lund string fragmentation parameters in the AMPT model, seems to give a good description of the spectra for all the considered particles at three energies in 0–5% central collisions. The kaon spectrum in the SM AMPT model underpredicts the data by a factor 2 at 7.7 GeV, which suggests that the SM AMPT model is not well suited to study kaon (strangeness) production at lower energies.

The comparisons of dN/dy as a function of collision centrality suggest that particle yields cannot be described simultaneously by the AMPT model for all the particles at the three energies. Pion and proton dN/dy are not described at 200 GeV while kaon dN/dy is not described at 7.7 GeV at all the centralities. The pion and proton dN/dy at 7.7 GeV are described by set B parameters; pion and kaon dN/dy at 27 GeV are described by default set C parameters while proton dN/dy are described by SM set A parameters; and kaon dN/dy at 200 GeV is described by default set A and SM set C parameters. In general, for most cases, it is observed that set C parameters with the largest $a = 2.2$ produce higher yields while set B parameters with the smallest $a = 0.5$ produce smaller yields of particles.

Comparisons of $\langle p_T \rangle$ as a function of centrality suggest that except for the pion $\langle p_T \rangle$ at 7.7 GeV (which is described at all centralities by default set C parameters), the AMPT model does not explain the data at all centralities for the three energies. The pion $\langle p_T \rangle$ is not explained at all by the AMPT model at 200 GeV. For other energies and particles, $\langle p_T \rangle$ as a function of centrality is only explained partially by the model. For these cases, the set A parameters, corresponding to 3 mb cross section with $a = 0.55$ and $b = 0.15 \text{ GeV}^{-2}$, mostly work better than the other two.

Comparisons of antiparticle-to-particle ratios as a function of centrality suggest that π^-/π^+ ratio is explained by the AMPT model at three energies and all centralities while K^-/K^+ and \bar{p}/p ratios are explained at 27 and 200 GeV but not at 7.7 GeV, where they are only partly described. The pion ratio does not distinguish between default and SM AMPT models. The kaon ratio favors SM; similarly, the proton ratio also favors the SM except at 200 GeV, where default AMPT works better.

Comparisons of mixed particle ratios as a function of centrality suggest that the K^\pm/π^\pm ratio at 7.7 GeV is not described well by any of the models at all centralities, except at the peripheral bins. This indicates that the production of kaons (strange particles) is not explained by the AMPT model at lower energies. At 27 and 200 GeV, these ratios are described by default and/or SM set C parameters, i.e., with a 10 mb parton cross section and $a = 2.2, b = 0.5 \text{ GeV}^{-2}$. The p/π^+ ratio is explained for all centralities at 7.7 and 27 GeV but for a few centralities at 200 GeV by the AMPT model. The model explains

TABLE II: Summary table for the performance of various sets in AMPT default and SM models for different observables presented. The \checkmark symbol represents that the particular set describes the data well (“-” symbol represents that the given set does not explain the data well at all energies as compared to other sets), * represents that the set describes the data partially, X (in “Remark” column) suggests that none of the sets could describe the data. The figures in the parentheses followed by the symbols represent the energy $\sqrt{s_{NN}}$ (GeV) where these sets are applicable.

Observable		AMPT Default			AMPT String Melting			Remark
		Set A	Set B	Set C	Set A	Set B	Set C	
p_T spectra (0–5%)	π^+	\checkmark (27, 200)	-	-	\checkmark (7.7, 200)	-	-	
	K^+	\checkmark (7.7, 27) * (200)	-	-	-	-	-	
	p	\checkmark (7.7, 27, 200)	-	-	\checkmark (7.7, 27, 200)	-	-	
dN/dy vs. $\langle N_{\text{part}} \rangle$	π^+	* (200)	-	-	-	* (200)	\checkmark (7.7, 27)	
	K^+	\checkmark (200)	-	\checkmark (27)	-	-	\checkmark (200)	X (7.7)
	p	\checkmark (7.7)	\checkmark (7.7)	\checkmark (7.7)	\checkmark (7.7, 27)	\checkmark (7.7) * (200)	\checkmark (7.7)	
$\langle p_T \rangle$ vs. $\langle N_{\text{part}} \rangle$	π^+	-	-	\checkmark (7.7)	* (27)	-	-	X (200)
	K^+	* (7.7, 200)	* (7.7)	* (7.7)	* (27, 200)	-	-	
	p	* (200)	-	-	* (7.7, 27)	* (7.7)	* (7.7)	
Ratios vs. $\langle N_{\text{part}} \rangle$	π^-/π^+	\checkmark (7.7, 27) \checkmark (200)	\checkmark (7.7, 27) \checkmark (200)	\checkmark (7.7, 27) \checkmark (200)	\checkmark (7.7, 27) \checkmark (200)	\checkmark (7.7, 27) \checkmark (200)	\checkmark (7.7, 27) \checkmark (200)	
	K^-/K^+	-	-	-	\checkmark (27, 200)	-	* (7.7)	
	\bar{p}/p	-	\checkmark (200)	-	-	-	* (7.7) \checkmark (27)	
	K^+/π^+	-	-	\checkmark (27, 200)	-	-	\checkmark (200)	X(7.7)
	K^-/π^-	-	-	\checkmark (27)	-	-	\checkmark (27, 200)	X(7.7)
	p/π^+	\checkmark (7.7, 27)	\checkmark (7.7)	\checkmark (7.7)	\checkmark (7.7, 27) * (200)	\checkmark (7.7) * (200)	\checkmark (7.7) * (200)	
Ratios vs. $\sqrt{s_{NN}}$ (0-5%)	\bar{p}/π^-	\checkmark (200)	* (7.7)	* (7.7) \checkmark (27)	-	* (7.7)	* (7.7)	
	K^+/π^+	* (27, 200)	* (27, 200)	* (27, 200)	* (27, 200)	* (200)	* (200)	At 7.7 GeV default model is closer to expt. data
	K^-/π^-	* (27, 200)	* (27, 200)	* (27, 200)	* (27, 200)	* (200)	* (27, 200)	
	p/π^+	\checkmark (7.7, 27) \checkmark (200)	* (7.7, 27)	* (7.7, 27)	\checkmark (7.7, 27) \checkmark (200)	\checkmark (7.7, 27) \checkmark (200)	* (7.7)	
\bar{p}/π^-	* (7.7, 200)	* (7.7, 27)	* (7.7, 27)	* (7.7)	* (7.7)	* (7.7, 200)		

the \bar{p}/π^- ratio for all centralities at all energies. It seems that both the default and SM models are favored by the p/π^+ ratio at $\sqrt{s_{NN}} \leq 27$ GeV while the default AMPT model is favored by the \bar{p}/π^- ratio for all centralities at the three energies.

The energy dependence of mixed particle ratios for 0–5% central collisions is also studied. The K^\pm/π^\pm ratio is not explained by the AMPT model at 7.7 GeV. At 27 and 200 GeV, the default AMPT model with all the three sets and SM with set A parameters describe the data. Thus, we again observe that the strangeness (kaon) production at $\sqrt{s_{NN}} = 7.7$ GeV is not explained by the AMPT model. In addition, the default model is in relatively closer agreement with the data at lower energies than the SM AMPT model. In the SM model, the parton density is quite dense as all the HIJING strings are converted to partons. Thus, the model with SM is expected to work well in high energy density regions. Our observation that it performs unsatisfactorily (and worse than default AMPT) at the lower energy of 7.7 GeV but gives progressively better predictions at higher energies supports the above statement. The energy dependence of p/π^+ ratio is better explained by default set A param-

eters and by SM set A and B parameters. The energy dependence of the \bar{p}/π^- ratio is not consistently described by any parameter set of either the default or SM model. However, the default AMPT can describe the ratio at the three energies with different sets, with the set A parameters results being closest to the data. These results, and also those from the energy dependence of particle yields, $\langle p_T \rangle$, and ratios in 0–5% central collisions, suggest that the default AMPT with set A parameters (3 mb cross section, $a = 0.55$, and $b = 0.15$ GeV $^{-2}$) is generally better than the other sets and also better than the SM version with any set. As mentioned earlier, by including the finite nuclear thickness of incoming colliding nuclei into the SM model might improve results at lower energies. Nevertheless, these results complement and are also in contrast to the previously established picture that elliptic flow v_2 is better described by the SM version. This also suggests that some more work might be needed to consistently describe all bulk properties of the system formed in heavy-ion collisions at different energies and centralities. The new quark coalescence is one of the steps towards that direction [30]. The results from this study provide input in constraining the models in a bet-

ter way and also understanding the particle production in heavy-ion collisions.

V. ACKNOWLEDGEMENTS

We thank Bedagadas Mohanty for suggestions and comments on the manuscript. A.N. acknowledges sup-

port from the IAS-NASI-INSA academies as part of the Science Academies' Summer Research Fellowship Program and the Physics Department, Panjab University Chandigarh. N.S. acknowledges the support of a DST-SERB Ramanujan Fellowship (D.O. No. SB/S2/RJN-084/2015). L.K. acknowledges the support of SERB Grant No. ECR/2016/000109.

-
- [1] J. Adams et al. (STAR Collaboration), Nucl. Phys. **A757**, 102 (2005).
- [2] K. Adcox et al. (PHENIX Collaboration), Nucl. Phys. **A757**, 184 (2005).
- [3] I. Arsene et al. (BRAHMS Collaboration), Nucl. Phys. **A757**, 1 (2005).
- [4] B. B. Back et al., Nucl. Phys. **A757**, 28 (2005).
- [5] E. Laermann and O. Philipsen, Ann. Rev. Nucl. Part. Sci. **53**, 163 (2003).
- [6] K. Rajagopal and F. Wilczek, arXiv hep-ph/0011333 (2000).
- [7] M. Stephanov, PoS **LAT2006**, 024 (2006).
- [8] J. Cleymans and K. Redlich, Phys. Rev. **C60**, 054908 (1999).
- [9] F. Becattini, J. Manninen, and M. Gazdzicki, Phys. Rev. **C73**, 044905 (2006).
- [10] A. Andronic, P. Braun-Munzinger, and J. Stachel, Nucl. Phys. **A772**, 167 (2006).
- [11] L. Kumar and D. Keane, Pramana **84**, 773 (2015).
- [12] L. Kumar (STAR), Nucl. Phys. **A862-863**, 125 (2011).
- [13] B. I. Abelev et al. (STAR Collaboration), Phys. Rev. **C81**, 024911 (2010).
- [14] B. Mohanty, Nucl. Phys. **A830**, 899C (2009).
- [15] M. Aggarwal et al. (STAR Collaboration), arXiv: p. 1007.2613 (2010).
- [16] L. Kumar (STAR), Nucl. Phys. **A904-905**, 256c (2013).
- [17] L. Kumar, Mod. Phys. Lett. **A28**, 1330033 (2013).
- [18] L. Adamczyk et al. (STAR Collaboration), Phys. Rev. **C96**, 044904 (2017).
- [19] L. Adamczyk et al. (STAR Collaboration), Phys. Rev. Lett. **112**, 032302 (2014).
- [20] L. Adamczyk et al. (STAR Collaboration), Phys. Rev. Lett. **112**, 162301 (2014).
- [21] L. Adamczyk et al. (STAR Collaboration), Phys. Rev. Lett. **113**, 052302 (2014).
- [22] L. Adamczyk et al. (STAR Collaboration), Phys. Rev. Lett. **121**, 032301 (2018).
- [23] L. Adamczyk et al. (STAR Collaboration), Phys. Rev. Lett. **116**, 062301 (2016).
- [24] L. Adamczyk et al. (STAR Collaboration), Phys. Rev. Lett. **110**, 142301 (2013).
- [25] L. Adamczyk et al. (STAR Collaboration), Phys. Rev. Lett. **120**, 062301 (2018).
- [26] L. Adamczyk et al. (STAR Collaboration), Phys. Rev. **C86**, 054908 (2012), 1206.5528.
- [27] L. Adamczyk et al. (STAR Collaboration), Phys. Rev. **C93**, 014907 (2016), 1509.08397.
- [28] Z.-W. Lin, C. M. Ko, B.-A. Li, B. Zhang, and S. Pal, Phys. Rev. **C72**, 064901 (2005), nucl-th/0411110.
- [29] L. Zhu, C. M. Ko, and X. Yin, Phys. Rev. **C92**, 064911 (2015), 1510.03568.
- [30] Y. He and Z.-W. Lin, Phys. Rev. **C96**, 014910 (2017), 1703.02673.
- [31] J. Xu and C. M. Ko, Phys. Rev. **C83**, 034904 (2011).
- [32] X.-N. Wang and M. Gyulassy, Phys. Rev. **D44**, 3501 (1991).
- [33] B. Zhang, Comput. Phys. Commun. **109**, 193 (1998).
- [34] B. Andersson, G. Gustafson, and B. Soderberg, Z. Phys. **C20**, 317 (1983).
- [35] B. Andersson, G. Gustafson, G. Ingelman, and T. Sjostrand, Phys. Rept. **97**, 31 (1983).
- [36] B.-A. Li and C. M. Ko, Phys. Rev. **C52**, 2037 (1995).
- [37] N. Fischer and T. Sjostrand, JHEP **01**, 140 (2017), 1610.09818.
- [38] Z.-W. Lin, Phys. Rev. **C90**, 014904 (2014).
- [39] B. Zhang, C. M. Ko, B.-A. Li, and Z.-w. Lin, Phys. Rev. **C61**, 067901 (2000).
- [40] Z.-w. Lin, S. Pal, C. M. Ko, B.-A. Li, and B. Zhang, Phys. Rev. **C64**, 011902 (2001).
- [41] B. I. Abelev et al. (STAR Collaboration), Phys. Rev. **C79**, 034909 (2009).
- [42] Y. Akiba et al. (E802 Collaboration), Nucl. Phys. **A 610**, 139c (1996).
- [43] L. Ahle et al. (E802 Collaboration), Phys. Rev. **C 57**, 466 (1998).
- [44] L. Ahle et al. (E866 Collaboration, E917 Collaboration), Phys. Lett. **B 476**, 1 (2000).
- [45] L. Ahle et al. (E802 Collaboration, E866 Collaboration), Phys. Rev. **C 60**, 044904 (1999).
- [46] L. Ahle et al. (E866 Collaboration, E917 Collaborations), Phys. Lett. **B 490**, 53 (2000).
- [47] S. Afanasiev et al. (NA49 Collaboration), Phys. Rev. **C 66**, 054902 (2002).
- [48] C. Alt et al. (NA49 Collaboration), Phys. Rev. **C 77**, 024903 (2008).
- [49] J. Randrup and J. Cleymans, Phys. Rev. **C74**, 047901 (2006), hep-ph/0607065.
- [50] Z.-W. Lin, Phys. Rev. **C 98**, 034908 (2018), 1704.08418.
- [51] C. Shen, G. Denicol, C. Gale, S. Jeon, A. Monnai, and B. Schenke, Nucl. Phys. A **967**, 796 (2017), 1704.04109.